Coordinated Use of Structure-Integrated Bistable Actuation Modules for Agile Locomotion

Satoshi Nishikawa, Yusuke Arai, Ryuma Niiyama, and Yasuo Kuniyoshi

***Abstract*—It is difficult to design agile soft-bodied robots owing to their inherent softness. To overcome this problem, we propose a structure-integrated bistable module that uses snap-through buckling for agile motions. First, we confirmed that a 0.05-m-long module was able to jump to 0.13 m high. Through investigation, we found a range of command parameters within which the module jumps consistently. Moreover, we showed that jumping performance had strong relation to the bending amplitude. Next, we induced a robot with two serially connected modules to roll forward and jump over an obstacle. In rolling, the robot became round for quick locomotion. In jumping, we found that buckling in one module induced buckling in the other module. The difference in buckling time between the two modules was shortened from the order of 0.1 s to the order of 0.01 s. This might be effective for error correction or useful for coordinated motions. These results show the effectiveness of the proposed structure-integrated bistable modules for making agile soft-bodied robots, and suggest ways of exploiting them.**

***Index Terms*—Soft material robotics, mechanism design, compliant joint/mechanism.**

I. Introduction

SOFT-BODIED robots have the potential to be robust and adaptable in changing and unpredictable environments such as disaster sites, as well as in daily life. Therefore, many soft-bodied robots have been developed [1]–[3]. However, soft-bodied robots have difficulty with agile motion because soft materials cannot transmit power efficiently and consume energy through deformation. Moreover, pneumatic actuators and shape-memory alloy (SMA) actuators used in soft robotics have low bandwidth. If their agility can be improved, soft-bodied robots will be able to jump over obstacles or avoid danger quickly.

High-speed large-force actuators might enable agile motion in soft-bodied robots. However, designing such an actuator is difficult because there is a trade-off between speed and force.

Manuscript received September 10, 2017; accepted December 26, 2017. Date of publication January 17, 2018; date of current version February 1, 2018. This letter was recommended for publication by Associate Editor H. Choi and Editor Y. Sun upon evaluation of the reviewers comments. This work was supported in part by JST ERATO under Grant JPMJER1501 and JSPS under Grant-in-Aid for Research Activity Start-up 15H06140. *(Corresponding author: Satoshi Nishikawa.)*

The authors are with the Department of Mechano-Informatics, Graduate School of Information Science and Technology, The University of Tokyo, Tokyo 113-8656, Japan (e-mail: nisikawa@isi.imi.i.u-tokyo.ac.jp; arai@isi.imi.i.u-tokyo.ac.jp; niiyama@isi.imi.i.u-tokyo.ac.jp; kuniyosh@isi.imi.i.u-tokyo.ac.jp).

This letter has supplementary downloadable material available at http://ieeexplore.ieee.org, provided by the authors. The Supplemental Material contains a video of simulation and robot experiments. This material is 25.8 MB in size.

Digital Object Identifier 10.1109/LRA.2018.2794617

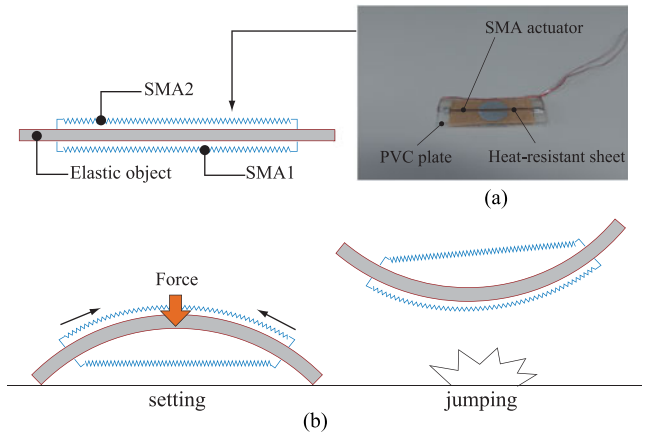

Fig. 1. Structure-integrated bistable module. (a) Bistable module. (b) Snap-through buckling motion.

For example, speed-reduction gears increase the force, but at the expense of speed. To overcome this trade-off, elastic elements can be used, which can exert a large force by instantaneous release of stored energy [4]. Stored energy in elastic tissue is essential in the jumping systems of insects [5]. They have trigger mechanisms for rapid release of stored energy. Another option for agile motion involves using chemical reactions [6]. However, these require a complex mechanism for dividing and mixing the chemicals and for igniting the mixture.

For agile motion, we focused on the bistable snap-through buckling mechanism [7]. This mechanism is simple and does not need locking parts; therefore, it is promising for low weight and high fault tolerance. Although some robots have used snap-through buckling, they had frames [8] or had only a single mechanism [9]. Frames prevent the exploitation of shape change, and deformability is one of the essential properties of soft-bodied robots. For example, a caterpillar-inspired soft-bodied robot realized a ballistic rolling motion by curling its body [10]. Moreover, robots can be made lighter if a structure-integrated mechanism is used without frames. In addition, coordinated work from multiple mechanisms can increase the modes of motion. Thus, we have previously proposed a structure-integrated bistable module (Fig. 1) and confirmed its bistable property and ability for jumping [11].

In the present letter, building on the above research, we investigate the effect of motion parameters of the structure-integrated bistable module. We also investigate dynamic motion by using multiple modules using shape changes and coordination. First, we present a bistable module and a corresponding simulation

model. Next, we report a single-module experiment using the simulation model and a real robot, to investigate the relation between motion generation parameters and performance. Then, we report a simulation of dynamic motions using multiple modules in combination, and experiments to demonstrate these motions using real robots with multiple modules. Finally, we discuss phenomena observed in the experiments involving the two-module robot.

II. Methods

A. Structure-Integrated Bistable Module

To enable a soft mechanism to perform dynamic motion, we proposed a module combining an elastic body plastic plate and an SMA actuator, as shown in Fig. 1(a). This structure is driven by SMA actuators on both sides of an elastic–plastic plate. Although simple, this mechanism is capable of generating an instantaneous force large enough to allow itself to jump. It can be compact thanks to its planar structure. Its structure-integrated design means that this mechanism can also change shape, permitting passive motions such as rolling.

We used SMA actuators for this module because they have a high force/weight ratio and are soft, and therefore compatible with soft-bodied [12]. There are some disadvantages to SMA actuators, including a slower extension speed than contraction speed, large errors caused by temperature variations which prevents repetitive operation, and hysteresis. Among these, we refined the slow extension speed associated with this mechanism. The extension of an SMA actuator was accelerated by supporting the SMA actuator on the opposite side of plate. In addition, by combining SMA actuators with a bistable mechanism, the module can achieve rapid motion.

In this study, Biometal Helix 150 (BMX 150; Toki Corporation) was used as the SMA actuator. This SMA actuator contracts by heating and extends by cooling. In the Biometal Helix 150, the SMA itself also serves as an electrical resistor, and contracts using heat generated by an electric current. Because this actuator is composed of a coiled SMA, its contraction ratio (approximately 50%) is higher than that of a linear SMA actuator. In this study, we used a polyvinyl chloride plate for the plastic structure and attached heat-resistant sheets to both sides to protect it from heat.

A bistable module with two SMA actuators can bend in one of two directions by contracting the SMA actuator on that side. It can also generate snap-through buckling by controlling both SMA actuators according to the following procedure. In a two-dimensional plane, the module consists of a central elastic body sandwiched between upper and lower SMA actuators (Fig. 1).

1) SMA 1 on the lower surface receives an electric current. The SMA contracts, causing the elastic body to deform into a convex arcuate shape
2) After this deformation, the electric current is stopped.
3) SMA 2 on the upper surface receives an electric current causing contraction. When the elastic body becomes almost straight, snap-through buckling occurs, caused by the restoring force of the elastic body.

Snap-through buckling generates an impact force between the module and the ground, making the module jump (Fig. 1(b)).

TABLE I
Specification of Bistable Module

Parameters	Value
Size [mm^3]	$20 \times 50 \times 0.2$
Mass [g]	1.2
Flexural modulus [kg/cm^2]	21 100 $\sim$ 35 200
Length of SMA [mm]	4
Voltage [V]	5

We preliminarily tested the snap-through buckling operation with several design patterns, to determine module parameters such as size, plastic plate thickness, and SMA length. Table I shows the physical properties of the bistable module used in this study.

B. Simulator

To investigate the behavior of the module and the energy change in the snap-through buckling mechanism, we constructed a simulation. We modeled the elastic body using a multi-body system. This model consisted of mass points connected with springs and dampers. The bending energy of an elastic body E_{elastic} is calculated as:

$$E_{\mathrm{elastic}} = \frac{1}{2}\sum_{i=2}^{n-1} k_{\mathrm{joint}}\theta_i^2. \tag{1}$$

Here, n is the number of mass points, k_{joint} is the rotating spring constant and θ_i is the angle formed by the $(i-1)$th, ith and $(i+1)$th mass-points. We defined θ_i so that $\theta_i = 0$ when three mass points are aligned on a straight line.

We modeled the collision between the elastic body and the ground using the penalty method. The normal force at the ith mass-point N_i is calculated as:

$$N_i = k_{\mathrm{ground}}(z_i) + c_{\mathrm{ground}}\dot{z}_i. \tag{2}$$

Here, k_{ground} and c_{ground} are constants, and z_i is the vertical distance between the ith mass-point and the ground. Friction F_{f} is calculated using N_i.

$$F_{\mathrm{f}} = \begin{cases} \min(\mu_{\mathrm{s}}N_i, F_{i,x}) & (|\dot{x}_i| < v_{\mathrm{th}}) \\ \mu_{\mathrm{d}}N_i & (|\dot{x}_i| \geq v_{\mathrm{th}}) \end{cases} \tag{3}$$

Here, μ_{s} is the static friction coefficient, μ_{d} is the dynamic friction coefficient, $F_{i,x}$ is the horizontal force on ith mass-point, and v_{th} is the threshold velocity for the determination of movement.

The SMA model was approximated using a spring–damper model whose natural length varies.

$$f_{\mathrm{sma}} = k_{\mathrm{sma}}(l - l_{\mathrm{natural}}) + c_{\mathrm{sma}}\dot{l}. \tag{4}$$

Here, f_{sma} is the tension in the SMA actuator, l is the length of the SMA actuator, l_{natural} is the natural length of the SMA actuator, k_{sma} is the spring constant and c_{sma} is the viscosity coefficient.

We used the electric current state of the SMA actuator to represent changes in the natural length l_{natural} using the following

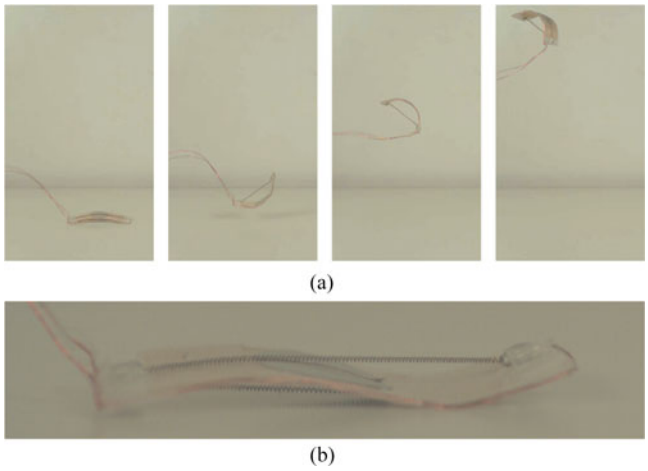

Fig. 2. Images of the single-module jumping experiment. (a) Snapshots of jumping. (b) Secondary buckling mode at the moment of snap-through buckling.

formula.

$$\text{Contraction} : \Delta l_{\text{natural}} = -v_{\text{contract}} \Delta t, \tag{5}$$

$$\text{Extension} : \Delta l_{\text{natural}} = p_{\text{sma}} f_{\text{sma}} \Delta t. \tag{6}$$

Here, v_{contract} is the contraction speed of the SMA actuator and p_{sma} is constant. The energy of the SMA actuator E_{sma} is calculated as:

$$E_{\text{sma}} = \frac{1}{2} k_{\text{sma}} (l - l_{\text{natural}})^2. \tag{7}$$

III. Single-Module Experiment

A. Experimental Setup

We examined the basic properties of the proposed structure using a single-module simulation and experiments. The experimental apparatus consisted of a bistable module, an Arduino Pro Mini (SparkFun Electronics, Inc.) and a PC. Both ends of each SMA actuator were connected to the Arduino using copper wire and FET shields. The output actuation voltage was 5 V. Motion was recorded using motion capture system OptiTrack (NaturalPoint, Inc.) at 240 Hz. We used six Prime 13 W cameras in this system. The diameter of each marker was 3 mm and its weight was less than 1 mg. The resolution of each camera was 1280×1024 pixels, and the field-of-view of each camera was 82° vertically and 70° horizontally. Mean error was less than 0.11 mm after calibration.

To generate jumping motion, we used motion commands based on the procedure explained in Section II-A. The parameters of the commands are time current is applied of each SMA T_1, T_2 and offset time t_{offset}, which is defined as the offset of the starting time of SMA 2 from the ending time of SMA 1.

B. Observation of Jumping

We observed the jumping behavior of the module using images captured by a high-speed camera (Phantom V1212; Vision Research, Inc.) at 1000 Hz. The module impacted the ground after snap-through buckling, causing it to jump (Fig. 2(a)). Before jumping, the module was in its secondary buckling mode (Fig. 2(b)).

TABLE II
Motion Command Parameters

Experiments	T_1 [s]	T_2 [s]	t_{offset}
Snapshots (experiment)	1.5	2.0	4.5
Change of t_{offset} (simulation)	1.5	2.0	0–10.0
Change of t_{offset} (experiment)	1.5	2.0	3.5–8.0
Change of T_1 (simulation)	0–2.5	2.0	6.0
Change of T_1 (experiment)	0.7–2.0	2.0	6.0

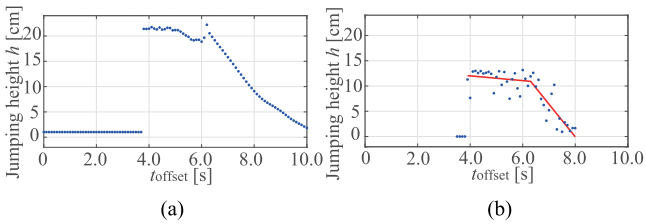

Fig. 3. Relation between the change of t_{offset} and jumping height. Red lines are piecewise linear regression lines $h = -0.5\, t_{\text{offset}} + 13.9$ and $h = -6.5\, t_{\text{offset}} + 51.6$ ($R^2 = 0.772$). Points on $h = 0$ are not used for regression. (a) Simulation. (b) Experiment.

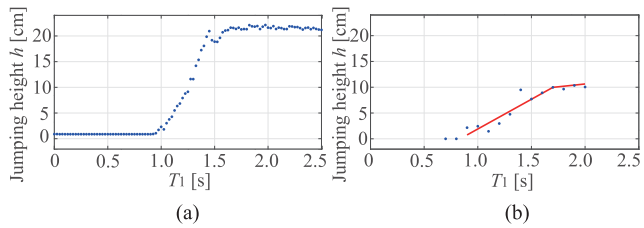

Fig. 4. Relation between the change of T_1 and jumping height. Red lines are piecewise linear regression lines $h = 11.5\, t_{\text{offset}} - 9.6$ and $h = 2.2\, t_{\text{offset}} + 6.2$ ($R^2 = 0.885$). Points on $h = 0$ are not used for regression. (a) Simulation. (b) Experiment.

C. Motion Command Parameters

We investigated the effect of each command parameter on the jumping height h, as shown in Table II. The simulation and experiment showed similar tendencies for t_{offset} or T_1 (Figs. 3, 4). This indicates that the simulation is useful for investigating the characteristics of the module.

Jumping height remained nearly constant at $4.0 \leq t_{\text{offset}} \leq 6.0$ [s] for both of the simulation and the experiment (Fig. 3). The difference in the jumping heights in the simulation and experiment might be caused by some loss related to friction or deformation. When looking at the energy transition in this stable period, rapid reduction of SMA 2's energy was observed in the simulation at the buckling time (Fig. 5). This energy release results in jumping. Comparing the energy transitions of different t_{offset} in the simulation, the energy of SMA 2 was almost highest at buckling time in this stable period. Buckling did not occur with small t_{offset} because the energy of SMA 2 dropped before it was a suitable shape for buckling, and buckling occurred before sufficient energy had accumulated with large t_{offset}.

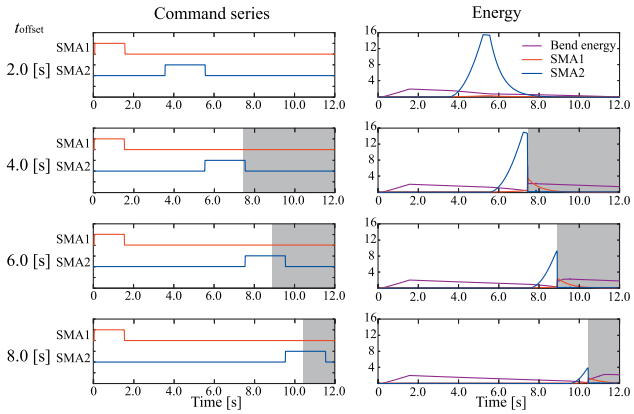

Fig. 5. Energy transitions with different t_{offset} in the simulation. The gray area indicates after buckling.

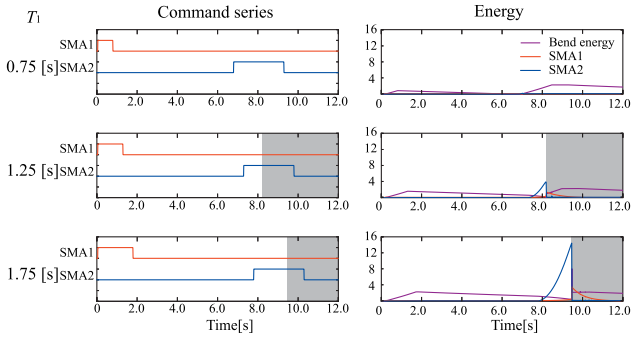

Fig. 6. Energy transitions with different T_1 in the simulation. The gray area indicated after buckling.

Jumping height remained nearly constant at $T_1 \geq 1.7$ [s] for both of the simulation and the experiment (Fig. 4). Comparing the energy transition of different T_1 in simulation, at small T_1, insufficient energy had accumulated in SMA 1 and buckling did not occur (Fig. 6). This indicates that jumps are consistently high when T_1 is above a certain value.

These results indicate that the proposed modules can consistently jump with a certain range of parameters. If boundary values for this range can be obtained from a small number of trials, it is possible to make a module jump consistently. The experimental results are regressed using piecewise lines to find the control parameters for the nearly constant jumping height (Figs. 3 and 4).

D. Relation Between Bending Amplitude and Jumping Performance

We examined the relation between bending amplitude and jumping performance, to evaluate the possibility of feedback control instead of feedforward timing control. Bending amplitude A_{b} was defined as the height of center of module at t_2. We defined t_{buckling} as the buckling timing.

Jumping height was consistent for a certain bending amplitude range (Fig. 7). The coefficient of determination of regression was $R^2 = 0.878$. This is larger than that of t_{offset}, $R^2 = 0.772$, indicating that feedback using bending amplitude is effective in reducing the error in the desired motion.

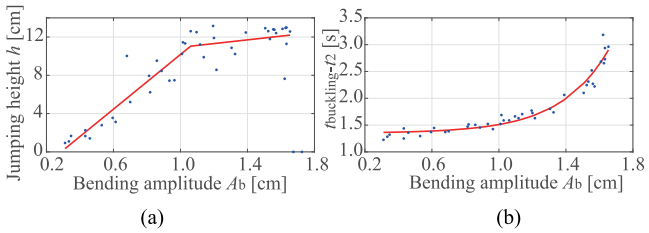

Fig. 7. Relations between change of bending amplitude and jumping height or buckling timing. Red lines in (a) are piecewise linear regression lines $h = 14.3A_{\mathrm{b}} - 4.1$ and $h = 1.9\,t_{\mathrm{offset}} + 9.0$ ($R^2 = 0.878$). Points on $h = 0$ are not used for regression. Red curve in (b) is a regression curve $t_{\mathrm{buckling}} - t_2 = 0.005e^{3.47A_{\mathrm{b}}} + 1.35$ ($R^2 = 0.950$). (a) Jumping height. (b) Buckling timing.

Buckling timing from t_2 was well fitted to the exponential function $t_{\mathrm{buckling}} - t_2 = 0.005e^{3.47A_{\mathrm{b}}} + 1.35$ ($R^2 = 0.950$).

IV. Two-Module Experiment

A. Experimental Setup

To investigate the characteristics of multiple modules using the simplest combination, we connected two modules serially. Modules were connected by tape to prevent free rotation.

B. Motions of the Two-Module Robot

First, we simulated the two-module motions. These motions were periodic and their parameters consisted of the period T_{p}, the length of time for which the current flows through each SMA actuator T_{ij}, and the time at which the current start flowing through each SMA actuator t_{ij}. Here, i is the name of module: A or B, and j is the number of the SMA actuator. We changed motion commands at random and extracted motions considered suitable for the target tasks. Target tasks were set as traveling horizontally or jumping over an obstacle. The target condition for the travelling task is large horizontal traveling distance in 0.5 s, and that for the jumping task is jumping higher than 0.05 m while traveling further than one body length. Next, we fabricated a real robot and made it move as in the simulation, using a trial-an-error procedure.

Most motions that met the large traveling distance target were forward-rolling motions, as shown in Fig. 8(a). All motions which met the jumping over an obstacle target were jumping with a change from S shape to reverse S shape, as shown in Fig. 8(b). Both motions were successfully replicated by the real robot (Figs. 9, 10, 11).

C. Adjustment of Jumping Motion

When jumping over an obstacle, small difference between the buckling timings of the two modules enables forward jumping. Therefore, we used the simulation to examine the relationship between the jumping motion and the difference between the buckling timing of the two modules. To change the buckling timing, we changed t_{diff}, defined as the time difference of t_{B1} from t_{A2}. The time difference was varied in the range $-1.0 < t_{\mathrm{diff}} < 1.0$. Here, we set values of all T_{ij}, $t_{\mathrm{offsetA}} = t_{\mathrm{A1}} - (t_{\mathrm{A2}} + T_{\mathrm{A2}})$ and $t_{\mathrm{offsetB}} = t_{\mathrm{B2}} - (t_{\mathrm{B1}} + T_{\mathrm{B1}})$ as 1.0 [s].

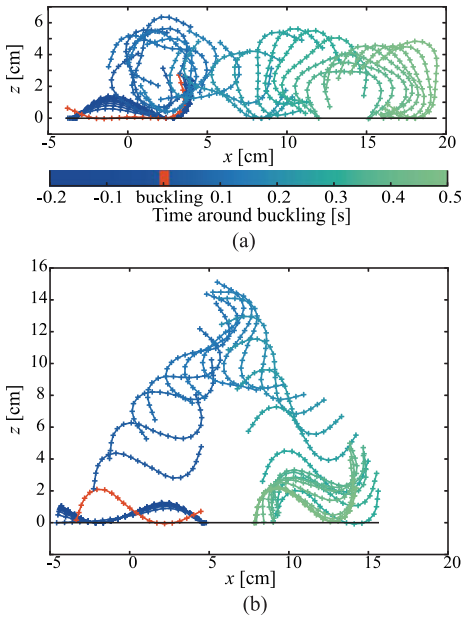

Fig. 8. Simulated motions of the two-module robot. (a) Forward rolling. (b) Jumping over an obstacle.

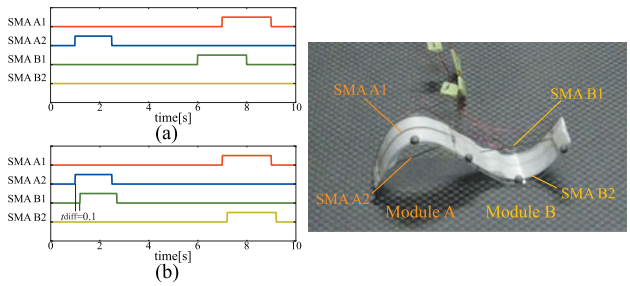

Fig. 9. Motion commands of two-module robot. (a) Command for forward rolling. (b) Command for jumping over an obstacle.

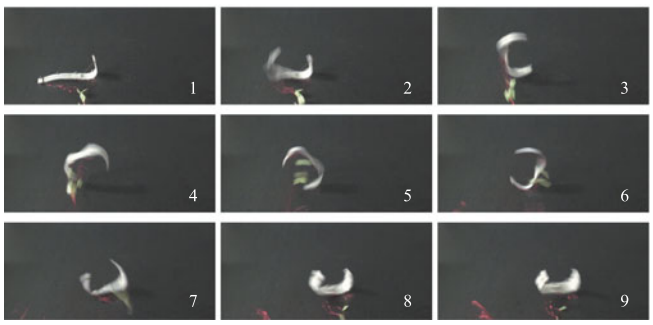

Fig. 10. Images of the forward-rolling motion. Frame rate is 30 Hz.

The jumping direction was changed by the sign of t_{diff} (Fig. 12). Different sign of t_{diff} showed different characteristics for the change of timing in simulation as follows. In positive values of t_{diff}, jumping distance varied depending on t_{diff}. For negative values of t_{diff}, jumping distance was almost the same for different amplitudes of t_{diff}. The reason for this asymmetric property is considered as follows. When upward buckling of module A occurred first (positive t_{diff}), the connection point was forced downward, and downward buckling of module B provided the main contribution to jumping. Therefore, a small

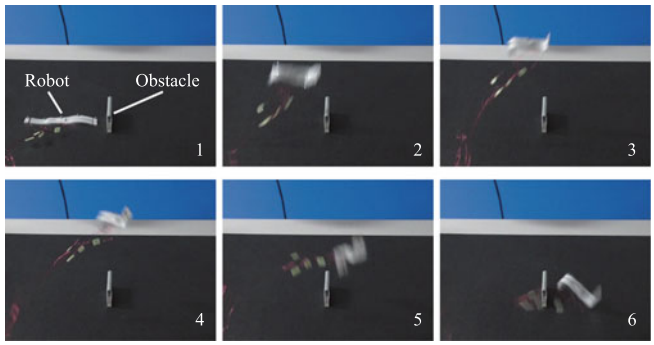

Fig. 11. Images of motion for jumping over an obstacle. Frame rate is 30 Hz.

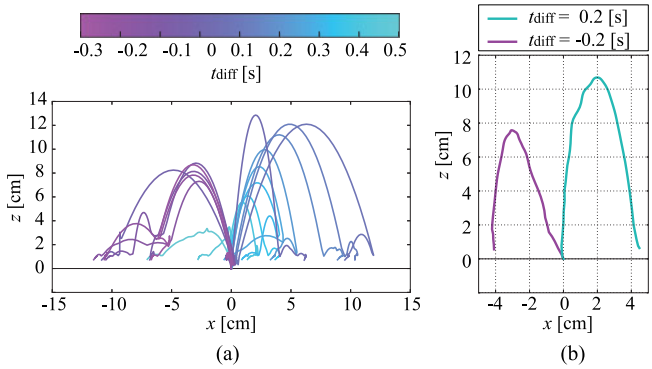

Fig. 12. Jumping trajectories with different t_{diff}. (a) Simulation. (b) Real robot.

difference in the timing of the buckling of module B influenced jumping performance. In contrast, when downward buckling of module B occurred first (negative t_{diff}), the connection point was forced upward, and the contribution of upward buckling of module A was reduced. Thus, this order stabilized the jumping performance regardless of the different timing of the buckling. In summary, the former case is effective to achieve higher jumping or to adjust the jumping performance by adjusting the timing of commands. In contrast, the latter case is effective for stabilizing jumping performance against timing errors in issued commands.

V. Discussion

A. Use of Shape Change

As shown in Figs. 8(a) and 10, the robot used its round shape to maintain its velocity. We also found other types of forward traveling motions. For example, there were motions involving single-sided buckling jumping, as shown in Fig. 13, or motions shown in Figs. 8(b) and 11. However, these motions resulted in less distance covered in 0.5 s than did rolling motion, although the number of bucklings was the same or larger. This indicates that an appropriate changes to the module shape would improve performance of robots in particular tasks.

B. Buckling Induction

We further investigated buckling in the jumping experiment described in Section IV-C. As shown in Fig. 14, even if the drive of SMA B2 was later than SMA A1, the buckling of module B occurred at almost the same time as that in module A, except

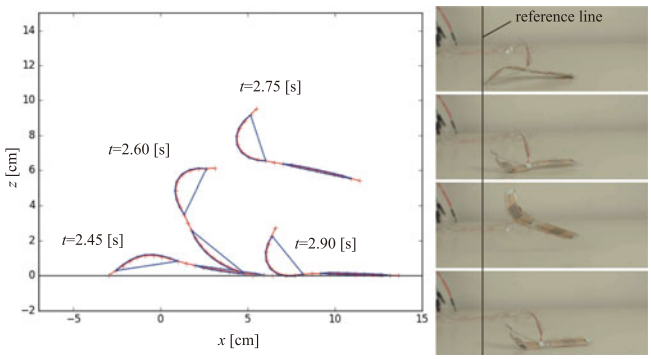

(a) (b)

Fig. 13. Single-sided buckling jump. (a) Simulation. (b) Real robot.

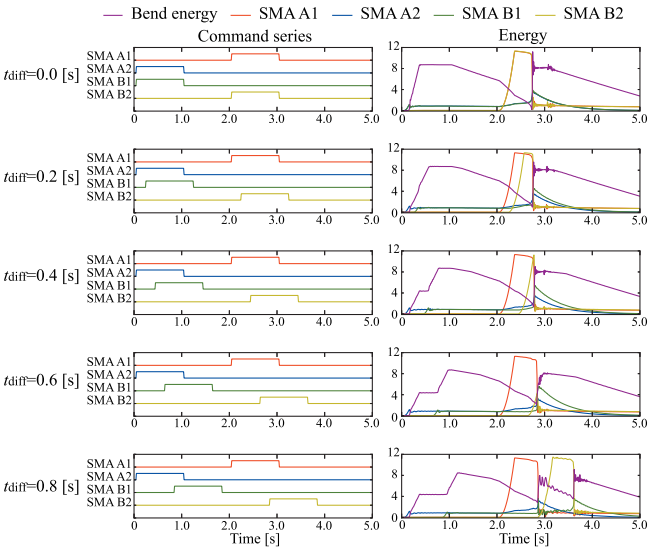

Fig. 14. Energy transition with buckling induction.

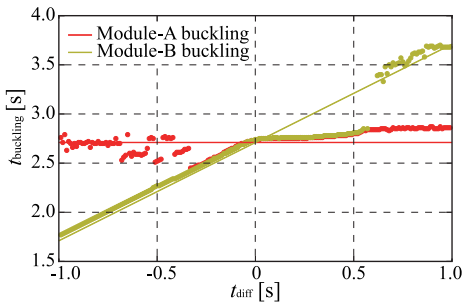

Fig. 15. Buckling timing of two modules. Lines indicate ideal buckling timing for a single module. Dots indicate the buckling timing of each module in the two-module robot.

when the difference was too large ($t_{\mathrm{diff}} = 0.8$ [s] in this case). Conversely, induction of buckling in module A was observed when drive of SMA B2 was earlier than SMA A1. The range for buckling induction was $-0.3 < t_{\mathrm{diff}} < 0.6$ (Fig. 15). We also conducted an experiment using a robot to validate these simulations. We set $t_{\mathrm{diff}} = 0.7$ [s]. We observed that buckling was induced in one module immediately after buckling of the other module (Fig. 16). In the jumping experiment in Fig. 12(b), the observed time difference of buckling was about 0.01 s, although

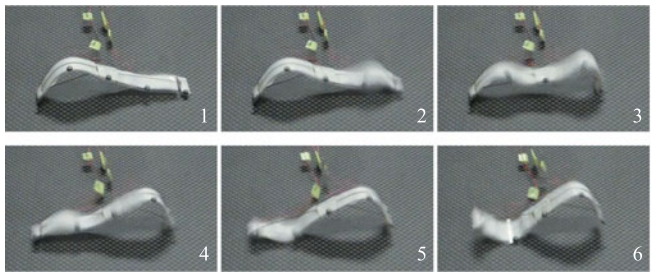

Fig. 16. Buckling induction in a real robot. Frame rate is 240 Hz. Buckling in the right module induced buckling in the left module.

the time difference between commands was 0.2 s. Buckling induction seems useful for coordinated motions or error corrections.

C. Limitations

Although we used a simple structure consisting of a plastic plate and SMA in this study, other materials might improve the physical performance of the module. Other promising materials are smart materials such as piezo-resistive material, piezoelectric material, and electro-active polymers whose bodies also change under external stimulation. Such materials have been used in soft robots and their structure-integrated nature might improve the compactness of the system.

The module has problems with repeatability in terms of fabrication and control. However, the error in fabrication could be addressed by individually tuning the commands required for a constant jumping height, as described in Section III-C. The repeatability for the control can be improved by using bending amplitude instead of timing, as described in Section III-D.

Because the robot was tethered to wires for electric current, the effect of these wires on its motion cannot be ignored. For example, the rotation of the robot was limited because the wires were twisted by the rotation. To reduce the effect of wires on the rotation, it could be useful to use a slip ring.

Another limitation of this study is that we did not consider the effect of the environment on the motions of the robot. To use the proposed modules in various environments, we need to investigate environmental effects such as the ground surface friction and inclination.

In this study, we evaluated only a serial connection of the modules. Thus, the orientation of the robots could not be controlled. To enable locomotion control including the orientation, a perpendicular combination might be effective.

VI. Conclusions

We proposed a structure-integrated bistable module using snap-through buckling. This module is intended to realize agile locomotion of soft-bodied robots using a combination of shape changing and coordination between multiple modules. In a single-module experiment, we confirmed that a 0.05 m module can jump to a height of 0.13 m. We also found that the timing of buckling commands can be adjusted to enable consistent jumping performance. In addition, we showed that consistency in jumping height can be also improved by using its bending

amplitude. Next, we investigated the characteristics of multiple modules using a robot with two serially connected modules. The robot achieved effective forward-traveling motion by making its body round and rolling. The robot achieved good jumping performance using a buckling combination. When jumping, induction of buckling was observed that shortened the difference between the buckling times of the two modules from the order of 0.1 s to the order of 0.01 s. This buckling induction might be useful for coordinated motions or error corrections. These results indicate the effectiveness of the proposed structure-integrated bistable module for use in agile soft-bodied robots, and suggest how it can be exploited. Future work may encompass methods for controlling modules for desired motions.

ACKNOWLEDGMENT

We thank Edanz Group (www.edanzediting.com/ac) for editing a draft of this manuscript.

REFERENCES

[1] R. F. Shepherd *et al.*, "Multigait soft robot," in *Proc. Nat. Acad. Sci.*, vol. 108, no. 51, pp. 20400–20403, 2011.

[2] S. Seok, C. D. Onal, K.-J. Cho, R. J. Wood, D. Rus, and S. Kim, "Meshworm: A peristaltic soft robot with antagonistic nickel titanium coil actuators," *IEEE/ASME Trans. Mechatron.*, vol. 18, no. 5, pp. 1485–1497, Oct. 2013.

[3] S. Kim, C. Laschi, and B. Trimmer, "Soft robotics: A bioinspired evolution in robotics," *Trends Biotechnol.*, vol. 31, no. 5, pp. 287–294, 2013.

[4] U. Scarfogliero, C. Stefanini, and P. Dario, "Design and development of the long-jumping "grillo" mini robot," in *Proc. IEEE Int. Conf. Robot. Autom.*, 2007, pp. 467–472.

[5] W. Gronenberg, "Fast actions in small animals: springs and click mechanisms," *J. Comparative Physiology A, Neuroethology, Sensory, Neural, Behavioral Physiology*, vol. 178, no. 6, pp. 727–734, 1996.

[6] M. T. Tolley *et al.*, "An untethered jumping soft robot," in *Proc. IEEE/RSJ Int. Conf. Intell. Robots Syst.*, 2014, pp. 561–566.

[7] A. Yamada, H. Mochiyama, and H. Fujimoto, "Kinematics and statics of robotic catapults based on the closed elastica," in *Proc. IEEE/RSJ Int. Conf. Intell. Robots Syst.*, 2007, pp. 3993–3998.

[8] Y. Sugiyama, A. Shiotsu, M. Yamanaka, and S. Hirai, "Circular/spherical robots for crawling and jumping," in *Proc. IEEE Int. Conf. Robot. Autom.*, 2005, pp. 3595–3600.

[9] A. Yamada, M. Watari, H. Mochiyama, and H. Fujimoto, "A jumping robot based on the closed elastica," in *Proc. Int. Symp. Micro-NanoMechatronics Human Sci.*, 2007, pp. 604–609.

[10] H.-T. Lin, G. G. Leisk, and B. Trimmer, "Goqbot: A caterpillar-inspired soft-bodied rolling robot," *Bioinspiration Biomimetics*, vol. 6, no. 2, 2011, Art. no. 026007.

[11] Y. Arai, S. Nishikawa, R. Niiyama, and Y. Kuniyoshi, "Compliant jumping mechanism with bi-stable structure," in *Proc. IEEE Int. Conf. Robot. Autom. Workshop Adv. Fabrication Morphological Comput. Soft Robot.*, 2017.

[12] S. Zhang, B. Liu, L. Wang, Q. Yan, K. H. Low, and J. Yang, "Design and implementation of a lightweight bioinspired pectoral fin driven by SMA," *IEEE/ASME Trans. Mechatron.*, vol. 19, no. 6, pp. 1773–1785, Dec. 2014.